THE JOURNAL OF PHYSICAL CHEMISTRY B

ARTICLE

pubs.acs.org/JPCB

Use of a Short Peptide as a Building Block in the Layer-by-Layer Assembly of Biomolecules on Polymeric Surfaces

Dewi P. Go,[†,‡] Andrew Hung,[§,¶] Sally L. Gras,[*,†,‡] and Andrea J. O'Connor[†]

[†]Particulate Fluids Processing Centre, Department of Chemical and Biomolecular Engineering, University of Melbourne, Parkville 3010, Victoria, Australia

[‡]Bio21 Molecular Science and Biotechnology Institute, University of Melbourne, Parkville 3010, Victoria, Australia

[§]School of Applied Sciences, RMIT University, Melbourne 3001, Victoria, Australia

[¶]Health Innovations Research Institute, RMIT University, Bundoora 3083, Victoria, Australia

Supporting Information

ABSTRACT: The incorporation of low molecular weight drugs and therapeutic peptides into multilayer films assembled via the layer-by-layer technique can potentially provide means to deliver small molecules to target sites and to tune their release. This study describes the use of both hydrophobic and electrostatic interactions to incorporate a tridecapeptide antiinflammatory hormone, α-melanocyte stimulating hormone (α-MSH), as a building block at the base of a multilayer assembly of hyaluronic acid (HA) and chitosan (CS) on poly(lactic-*co*-glycolic acid) (PLGA) surfaces. A range of switching layers, including a neutral lipid, dioleylphosphatidylcholine (DOPC), a negatively charged lipid mixture DOPC/dioleylphosphatidylserine (DOPS) and a negatively charged polysaccharide, HA, were investigated for their ability to support subsequent HA and CS layers. Molecular dynamics simulations were performed to examine the structure and surface chemistry of α-MSH in solution and on surfaces to provide insights into the conditions most likely to support multilayer assembly. The multilayer assembly was stable at physiological pH and was successfully applied to particulate systems.

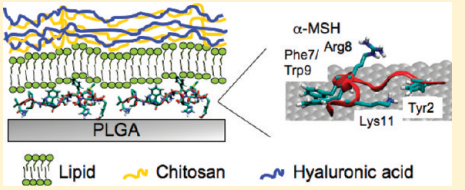

1. INTRODUCTION

Layer-by-layer (LbL) assembly is a versatile technique that enables multilayer films to be assembled via the subsequent deposition of materials with complementary chemical interactions.[1] A range of interactions including electrostatic attraction, hydrogen bonding, DNA hybridization, chemical reactions and hydrophobic interactions have been used to produce multilayer films. Such diversity allows a broad range of materials, including synthetic or biological polymers (charged and uncharged), inorganic or metal nanoparticles, proteins and small molecules, to be used to fabricate an array of functional LbL materials for various applications, most notably in the areas of biomaterials, drug delivery and tissue engineering.[2−6] We have recently used the LbL technique to deliver basic fibroblast growth factor (bFGF) utilizing the strong and well-characterized interaction between this growth factor and the highly sulfated polysaccharide heparin; embedding the growth factor within layers of polysaccharides to slow the rate of growth factor release over a period of 60 days.[7]

The properties of many newly developed drugs present a challenge for the future development of the LbL technique, as many are either small and hydrophobic or short peptide derivatives with limited charge.[8,9] The diffusion of such small molecules through LbL films means that they cannot be adequately and directly incorporated within the layers, offering limited control over their release.

One approach to overcome this problem is to load small molecules with low charge density into preformed capsules or films.[10,11] The loading mechanism is typically by diffusion through the pores within the LbL films and often results in a burst release within the first 48 h, as the molecules diffuse back through these pores. Another solution is to couple small drugs or peptides to a larger polyelectrolyte. This strategy has been used, for example, to tether an antiinflammatory tridecapeptide, α-melanocyte stimulating hormone, to poly-L-glutamic acid[12] and to encapsulate an antitumor drug, thiochoraline, in liposomes.[13] Such conjugates allow the assembly of stable multilayers via the LbL technique.

The use of small peptides directly as building constituents within an LbL assembly has proved challenging. Successful incorporation of oligopeptides directly within the LbL process is suggested to partly depend on the chain length and the peptide charge.[14] The instability of layers formed by short poly-L-glutamic acid (M_w 1.5−3 kDa) and poly-L-lysine (M_w 3.8 kDa) supports this hypothesis.[15]

Recently, anticancer peptides comprising 36 amino acids with nine positively charged residues and the small antibacterial peptide defensin, comprising 40 amino acids with five positively

Received: September 15, 2011
Revised: November 8, 2011
Published: December 20, 2011

charged residues, have been shown to interact electrostatically with polyanions to form a stable film with peptide release recorded over a period of 7 days.[16,17] Similarly, polypeptides with 32 amino acids specifically designed to comprise either 16 positively charged or negatively charged residues were successfully used as building blocks to construct hollow capsules via the LbL technique.[18] These studies represent a significant milestone in the fabrication of polypeptide films and control of peptide release via incorporation within multilayer constructs, utilizing both electrostatic and specific short-range interactions such as van der Waals forces and hydrogen bonds.

The anti-inflammatory human hormone α-melanocyte stimulating hormone (α-MSH; Ac-SYSMEHFRWGKPV-NH_2) is a suitable model peptide for potential incorporation within an LbL assembly, as it has features typical of many newly developed drugs. The 1.6 kDa peptide has 13 amino acid residues that are known to modulate the production of inflammatory cytokines in both *in vitro* and *in vivo* models of inflammation.[12,19] This peptide consists of mostly hydrophobic and neutral residues, with three charged residues randomly distributed along the backbone, Glu^5, Arg^8, and Lys^{11}, which contribute to a net charge of +1 at physiological pH. Previously, α-MSH has been conjugated to poly-L-glutamic acid, which was then used with oppositely charged poly-L-lysine to create bioactive coatings with antiinflammatory properties on tracheal prostheses and dental implants.[19,20] It is not clear, however, whether α-MSH can be incorporated without modification within an LbL assembly.

We have previously shown that α-MSH can be adsorbed directly onto the surface of the biodegradable polymer, poly(lactic-*co*-glycolic acid) (PLGA), via hydrophobic interactions.[21] In this study, we probe the structure of α-MSH in solution and upon binding to PLGA using spectroscopic techniques and molecular dynamics (MD) simulations with the goal of determining the optimum conditions for stable LbL deposition. MD has previously provided insights into a number of aspects of the LbL technique including polyelectrolyte complexation and the relationship between electrostatic interactions, hydrophobic interactions, hydrogen bond formation and secondary structure, all of which ultimately affect film stability.[3,22] Multilayer constructs were initially studied here on a planar system and MD was used to simulate the molecular arrangement of α-MSH on a model hydrophobic surface to determine the optimal configuration for use in the subsequent LbL assembly. Optimal layering conditions were translated to a three-dimensional construct of particles where the multilayers will potentially allow tunable release of α-MSH to modulate inflammation resulting from biomaterials and tissue engineering implants.

2. MATERIALS AND METHODS

2.1. Quartz Crystal Microbalance Measurements. Quartz crystal microbalance (QCM) measurements were performed to assess biomolecule binding to a 2D poly(lactic-*co*-glycolic) acid (PLGA; 75/25 Purasorb PDLG, MW ~95 000 Da, PURAC Biochem, Gorinchem, Holland) film.

2.1.1. Preparation of PLGA Films. Gold-coated 5 MHz AT-cut quartz crystals (Q-Sense AB, Västra, Frölunda, Sweden) were soaked with dioxane (Fluka, Buchs, Switzerland) for 1 min followed by cleaning with a mixture of purified water (Millipore Simplicity unit, Molsheim, France, purified to a resistivity of ≥18.2 MΩ.cm), ammonia (Ajax Finechem, Auckland, New Zealand) and hydrogen peroxide (Asia Pacific Specialty Chemicals, Auckland, New Zealand) at a volumetric ratio of 5:1:1 at 75 °C for 5 min. The crystals were then rinsed thoroughly with purified water followed by ethanol (Chem Supply, Gillman, SA, Australia). The crystals were immersed in a 5 mM solution of 1-ethyl-3-mercaptopropionate (SAFC, St. Louis, MI) in ethanol for 12 h to prepare for PLGA spin coating. PLGA films were formed by spin coating a solution of 1% (w/v) PLGA in dimethyl carbonate (Sigma Aldrich, St. Louis, MI) on the crystals for 2 min at 3000 rpm and annealing for 2 h at 75 °C on a hot plate.

To investigate the integration of α-MSH between polyelectrolyte layers, PLGA-coated crystals were first aminolyzed by immersion in a solution of 3% (w/v) 1,6-hexanediamine (Sigma Aldrich, MI) in isopropanol (Merck, Kilsyth, Australia) for 30 min at room temperature. The aminolyzed crystal was rinsed three times with purified water at 0 °C, soaked for a further hour in purified water at 0 °C, dried under vacuum over silica gel for 12 h and stored in a desiccator over silica gel until further use. For other experiments, the PLGA-coated crystals were not aminolyzed. The treated or untreated crystals were then placed in the analytical chamber of a Q-Sense D300 (Q-Sense AB, Västra, Frölunda, Sweden).

2.1.2. Layer-by-Layer Assembly on Planar Surface. A range of biomolecule solutions were prepared for this study. The α-MSH peptide (Ac-SYSMEHFRWGKPV-NH_2) was custom synthesized by CS Bio (Menlo Park, CA) with >95% peptide purity and the peptide mass was confirmed by mass spectrometry. The peptide was dissolved at a concentration of 50 μg/mL in either 10 mM 2-(*N*-morpholino)ethanesulfonic acid buffer (MES buffer; Research Organics, OH) which had been adjusted to pH 5.5 with 5 M NaOH or in 10 mM Tris buffer (Sigma Aldrich, MI) which had been adjusted to pH 9 with 1 M hydrochloric acid (Merck, Darmstadt, Germany). A stock solution of chitosan (CS; medium molecular weight CS, viscosity 286 cP, Lot number 07523MA, Sigma Aldrich) was prepared at a concentration of 5 mg/mL in 0.1 M acetic acid (BDH Laboratory Supplies, Poole, England). CS and hyaluronic acid (HA; molecular weight 1.6 MDa, Lifecore Biomedical, Chaska, MN) were both prepared at a concentration of 50 μg/mL in 10 mM MES buffer at pH 5.5. The cross-linking agent was prepared by dissolving 50 mg/mL of 1-ethyl-3-(3-dimethylaminopropyl)carbodiimide hydrochloride (EDC; Sigma Aldrich) and 100 mg/mL of *N*-hydroxysuccinimide (NHS; Sigma Aldrich) in dimethylformamide (DMF; BDH Laboratory Supplies, Poole, England). Ten minutes prior to adsorption, the cross-linking solution was added to the HA solution at 1% (v/v) to start the formation of the amine reactive intermediate product, NHS-ester.[23]

To study the adsorption of lipids on the α-MSH-coated PLGA, lipid was adsorbed from unilamellar liposomes suspended in aqueous buffer. The unilamellar liposomes were prepared by evaporating chloroform (Chem Supply, South Australia, Australia) from lipid solutions under nitrogen for 1 h to yield 2.5 mg of zwitterionic lipid [1,2-dioleoyl-*sn*-glycero-3-phosphocholine (DOPC), Avanti Lipids, AL] or 2.5 mg of negatively charged DOPC:DOPS [1,2-dioleoyl-*sn*-glycero-3-(phospho-L-serine) (DOPS), Avanti Lipids] at a ratio of 4:1. The dried lipids were then hydrated with 1 mL of MES or TRIS buffer depending on the desired pH for layering. Each solution was extruded through 50 nm polycarbonate filters (Whatman, ME) 31 times to obtain liposomes of monodisperse size.[24] The resulting liposomes were then diluted to 1 mg/mL for layering on the QCM crystals.

Once the baseline was obtained, α-MSH solution in either 10 mM Tris buffer at pH 9 or 10 mM MES buffer at pH 5.5 was

used to assemble the initial layer on PLGA-coated surface. The switching layers were assembled by introduction of either (1) HA in 10 mM MES buffer at pH 5.5 or (2) DOPC in 10 mM Tris buffer at pH 9 or 10 mM MES buffer at pH 5.5 depending on the pH of α-MSH adsorption or (3) DOPC/DOPS in 10 mM MES buffer at pH 5.5. Once the switching layers were formed, the multilayer films were continued by alternate adsorptions of CS and HA until the desired number of layers were formed. All HA solutions used for the layering process were already activated by the cross-linking agents as described above. The desired solutions were introduced and incubated within the measurement chamber until no further change in the frequency was observed, indicating that equilibrium had been reached. Samples were rinsed to remove nonadsorbed biomolecules with the same buffer used for loading before the introduction of a new solution for the next layer. Each time a new buffer was used, a new baseline was established. Measurements were collected at the fundamental frequency of 5 MHz as well as the third, fifth, and seventh overtones (14.9, 24.9, and 34.9 MHz, respectively). The temperature within the QCM chamber was kept constant at 23.5 °C. The masses of materials (m, ng/cm^2) adsorbed on the PLGA surface were estimated using the Sauerbrey equation (eq 1)

$$m = c\Delta F \quad (1)$$

where c is a constant 17.7 ng/(cm^2 Hz) and ΔF is the change of frequency due to the deposition of materials (Hz).[25]

2.2. Production of PLGA Microspheres. PLGA microspheres were produced using an oil-in-water emulsion and solvent evaporation technique as described previously.[7,26] Briefly, a 10% (w/v) solution of PLGA was prepared in dichloromethane (DCM; Merck, Australia). The polymer solution was emulsified in a 1% (w/v) poly(vinyl alcohol) solution (PVA; $M_w \sim 78\,000$ Da, 88% hydrolyzed, Polysciences Inc., USA) at 1500 rpm using an IKA RW 20 overhead stirrer (IKA Werke GmbH, Staufen, Germany) with a radial turbine impeller. The emulsion was stirred overnight to allow most of the DCM to evaporate, resulting in polymer precipitation and the formation of solid microspheres. The resultant microspheres were collected by centrifugation at 5250 g for 5 min and washed five times with purified water. The microspheres were then air-dried for 24 h under atmospheric conditions.

2.3. Fourier Transform Infrared Microscopy. The adsorption and the secondary structure of α-MSH on PLGA microspheres was probed by Fourier transform infrared (FTIR) microscopy. Loaded and unmodified PLGA microspheres were mounted on EZ-Spot Micro Mount sample slides (Thermo Scientific, USA). FTIR spectra were collected on a Hyperion 3000 Focal Plane Array (Bruker Optics Inc., USA) in reflectance mode at a spectral resolution of 4 cm^{-1} with 128 scans coadded using the Bruker Opus 6.5 software (Bruker Optics Inc., USA). The data were collected between 1600 cm^{-1} and 1840 cm^{-1} in the Amide I region and smoothed by using a weighted average of five data points. This research was undertaken on the infrared microspectroscopy beamline at the Australian Synchrotron, Victoria, Australia.

2.4. Circular Dichroism. Far-ultraviolet circular dichroism (CD) spectra were collected on a J-815 CD spectrometer (Jasco, Inc., Easton, MD) using a 1 mm path length quartz cuvette. The CD spectra of 100 μg/mL α-MSH were collected in 10 mM TRIS buffer at pH 9 and in 10 mM MES buffer at pH 5.5. The structure of the α-MSH peptide was also assessed following adsorption and desorption from a PLGA surface. A 150 mg sample of the PLGA microspheres was incubated with 3 mL of 250 μg/mL α-MSH solution in 10 mM Tris buffer at pH 9 for 2 h to promote adsorption. Once loaded, α-MSH was released into 1 mL of purified water at pH 7 for 72 h at 37 °C. The suspension was centrifuged at 9000g for 3 min. The volume of the supernatant containing α-MSH was reduced to 100 μL using a Centrivap concentrator (Labconco, Thermo Scientific, Australia) at 45 °C to increase the signal intensity sufficiently to record a meaningful spectrum. Water was selected as the release medium as its pH is close to physiological pH and the presence of salt would cause significant scattering following peptide release and buffer concentration prior to CD spectroscopy. The CD spectrum of fresh α-MSH was also determined in water for comparison. The temperature of all samples was kept constant at 23 °C during CD measurements using a circulating water bath. Spectra were collected between 185 and 260 nm, at a 0.1 nm interval and scanning rate of 50 nm/min. Each spectrum was the average of 6 scans. Deconvolution of the CD spectra was performed using the DICHROWEB online server using the CDSSTR algorithm.[27,28]

2.5. Molecular Dynamics Simulations. Simulations of α-MSH (with acetylated N-terminus and amidated C-terminus) in solution were constructed with the peptide placed in a rectangular simulation box of 40 Å^3, solvated with ~2100 simple point charge (SPC) water molecules.[29] For simulations at pH 9 or 5.5, 1 or 2 Cl$^-$ ions respectively were included in the solvent in order to ensure overall charge neutrality. For simulations at both pH values, α-MSH was modeled with charged basic and acidic side chains. At pH 9, the His^6 side chain was protonated only at the Nε^2 position (neutral residue), while at pH 5.5, both the Nε^2 and Nδ^1 positions were protonated (+1 charged residue). For both pH 9 and 5.5, six independent simulations were performed, with different starting peptide conformations. These consist of a fully extended strand (Figure S1A in the Supporting Information), an ideal α-helix (Figure S1C), two compact random coils (Figure S1D,E), and two extended random coils (Figure S1F,G). The latter four structures were obtained by using the Prelude and Fugue server to predict α-MSH conformations[30] and correspond to four low-energy structures as determined by the scoring function of this method.

In order to study the adsorption of α-MSH on PLGA, we approximate the polymer surface as a simple hydrophobic slab consisting of united-atom methyl ($-CH_3$) groups, which serve as a model of surface-exposed lactide methyls. The validity of this model and the possible influences of surface-exposed hydrophilic groups are discussed in section 3.5. Simulations of α-MSH adsorption onto a hydrophobic surface were constructed with the peptide initially placed approximately 6 Å above a uniform, flat impenetrable surface. The hydrophobic surface is approximated as two layers 13 Å apart, each consisting of a single layer of united-atom CH_3 particles arranged in a hexagonal lattice, with nearest-neighbor distances of 2.88 Å. This setup is shown in Figure S1B. The simulation cell was solvated with ~5300 SPC water and 1 or 2 Cl$^-$ counterions for pH 9 and 5.5, respectively, except for the space between the hydrophobic slabs. Simulations were performed at pH 9 and 5.5 with protonation states as described above. For both pH conditions, six independent simulations were performed with starting peptide conformations identical to those described above (Figure S1).

Molecular dynamics simulations were performed under constant particle number, pressure, and temperature (NPT) conditions using GROMACS version 4.5[31−34] and the GROMOS96 force field[35] with the 53A6 parameter set.[36,37] The simulation

trajectories were integrated using time steps of 2 fs. Particle mesh Ewald (PME) summation was employed for evaluation of long-range electrostatics,[38] while a cutoff radius of 1.0 nm was specified for short-range nonbonded interactions. Covalent bond lengths were constrained via the LINCS algorithm.[32] The simulation systems were maintained at 300 K and 1 bar using Berendsen temperature and pressure coupling.[39] Analyses of MD trajectories were performed using the GROMACS suite of analysis tools. Visualization of molecular graphics was performed using Visual Molecular Dynamics (VMD).[40]

A total of 24 simulations were performed: six each for α-MSH in solution and at a hydrophobic surface, at pH 9 and 5.5. For the solution systems, trajectories of 600 ns were collected for each of the simulations, while for the surface-adsorption systems, trajectories of 500 ns were collected for each simulation. Details of the simulations performed are summarized in Table S1 in the Supporting Information.

2.6. Layer-by-Layer Assembly of Biomolecules on PLGA Microspheres. PLGA microspheres (10 mg) were first coated with α-MSH by immersion in 1 mL of a 50 μg/mL α-MSH solution in 10 mM Tris buffer at pH 9 for 2 h at 37 °C with constant mixing at 90 rpm (Dynamica Intellimixer, Thermoline Scientific, Melbourne, Australia). HA and CS solutions in 10 mM MES buffer at pH 5.5 with a concentration of 200 μg/mL were used for coating the higher surface area of PLGA in the microsphere system compared to the 2D quartz crystal. Similarly, solutions of 2.5 mg/mL of zwitterionic liposomes in 10 mM Tris buffer at pH 9 and negatively charged liposomes in 10 mM MES buffer at pH 5.5 were used for layering. Activated HA and CS molecules were deposited for 30 min each whereas the lipids were allowed a longer period of 1 h to ensure maximal binding was achieved for each layer, based on preliminary observations from the QCM study. All layering was performed in 1.7 mL polypropylene microtubes (Eppendorf, NY) in a rotating device (Dynamica Intellimixer, Thermoline Scientific, Melbourne, Australia) at 90 rpm at room temperature. The microspheres were recovered by centrifugation at 9240*g* for 3 min after each layering step and rinsed with 1 mL of the loading buffer to remove unbound molecules. This washing step was repeated twice.

2.7. Confocal Scanning Laser Microscopy. PLGA microspheres were coated with α-MSH by adsorption from a solution of 50 μg/mL α-MSH at pH 9. Fluorescent liposomes were prepared by adding fluorescent lipid [1-oleoyl-2-[6-[(7-nitro-2-1, 3-benzoxadiazol-4-yl)amino]hexanoyl]-*sn*-glycero-3 phosphocholine (NBD-PC), Avanti Lipids] previously dissolved in chloroform during the formation of the DOPC and DOPC/DOPS liposomes to give a total of 10% labeled lipids in the liposome preparations. Samples of CS were labeled with either rhodamine B (Rhd; Sigma Aldrich, USA) or Alexa Fluor 488 (AF488; Invitrogen, Eugene, OR) following the manufacturer's instructions. A Slide-A-Lyser Dialysis cassette (Extra Strength, molecular weight cutoff of 10 000 Da, 3−12 mL capacity, Thermo Scientific, Rockford, IL) was used to separate the unreacted labeling reagent from the labeled CS according the manufacturer's protocol.

PLGA microspheres were layered with α-MSH-DOPC$^{\text{NBD-PC}}$-(CS-HA)$_5$, α-MSH-DOPC/DOPS$^{\text{NBD-PC}}$-(CS-HA)$_5$, and α-MSH-HA-CS$^{\text{Rhd}}$-(HA-CS)$_3$-HA-CS$^{\text{AF488}}$-HA as described earlier. Confocal laser scanning microscopy was carried out on a LSM 5 Pascal microscope equipped with a Neofluor 40× 1.30 DIC M27 oil objective lens (Carl Seiss, Hamburg, Germany). A sample of LbL-coated PLGA microspheres was air-dried and placed in a droplet of oil (518 F Seiss Immersol, Hamburg, Germany) on a microscope slide for imaging.

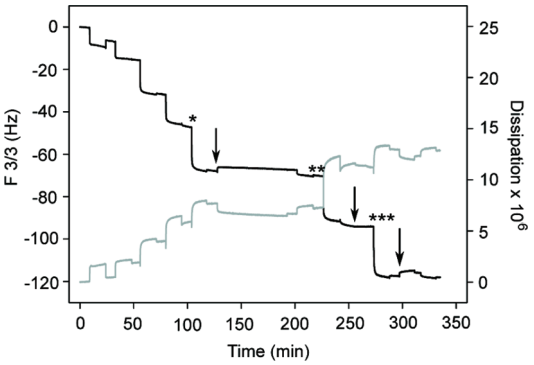

Figure 1. Frequency (black line) and dissipation (gray line) changes during layer-by-layer buildup of biomolecules on a 1,6-hexanediamine-aminolyzed PLGA substrate in the presence of cross-linking agents EDC and NHS. Five alternate CS and HA layers were deposited first. α-MSH peptide (shown by arrow) was then added at 130 min after a negatively charged HA layer (*), at 250 min after a positively charged CS layer (**), and at 300 min again after a negatively charged HA layer (***).

3. RESULTS AND DISCUSSION

3.1. Embedding of α-MSH into a Multilayer Film. We first set out to determine whether α-MSH could be directly incorporated within the middle layers of a biomolecule assembly consisting of the negatively charged polyelectrolyte hyaluronic acid (HA) and the positively charged polyelectrolyte chitosan (CS). A stable multilayer film comprising HA and CS was successfully assembled on an aminolyzed PLGA-coated QCM electrode at pH 5.5, where the polyelectrolytes are highly charged, as previously reported.[23] Under these conditions, HA will be negatively charged and CS positively charged as the pK_a of these biomolecules occur at ∼2.5 and 6.1, respectively.

Figure 1 shows the change in the frequency and dissipation during the multilayer build up as determined by QCM. This technique can detect minute changes in mass as small as ∼10 ng due to changes in the resonance frequency of an electrode. As the isoelectric point of α-MSH is ∼10, the peptide is expected to be positively charged at pH 5.5 due to the protonation of the amine groups on the arginine and lysine residues at positions eight and eleven (Figure 2). It was initially expected that the peptide could bind to a surface of opposing charge via electrostatic interactions but α-MSH did not bind to the negatively charged HA surface, as shown by the near-constant frequency and dissipation on α-MSH addition in Figure 1. Similarly, no α-MSH adsorbed on the positively charged CS surface, where the repulsion between like charges is expected to prevent adsorption.

The lack of adsorption of α-MSH to HA- and CS-coated surfaces necessitates another means of peptide loading, as is predicted for many small drugs and peptides. Our finding is consistent with observations that a small positively charged antibiotic, gentamicin, could not easily be incorporated within polyelectrolyte layers by electrostatic interactions.[41] Both gentamicin and α-MSH are likely to diffuse from the polyelectrolyte surface during assembly, resulting in the failure of stable film growth. Recent studies reporting the successful assembly of therapeutic peptides all involve polypeptides that are at least 3 times the length and 5 times more highly charged than

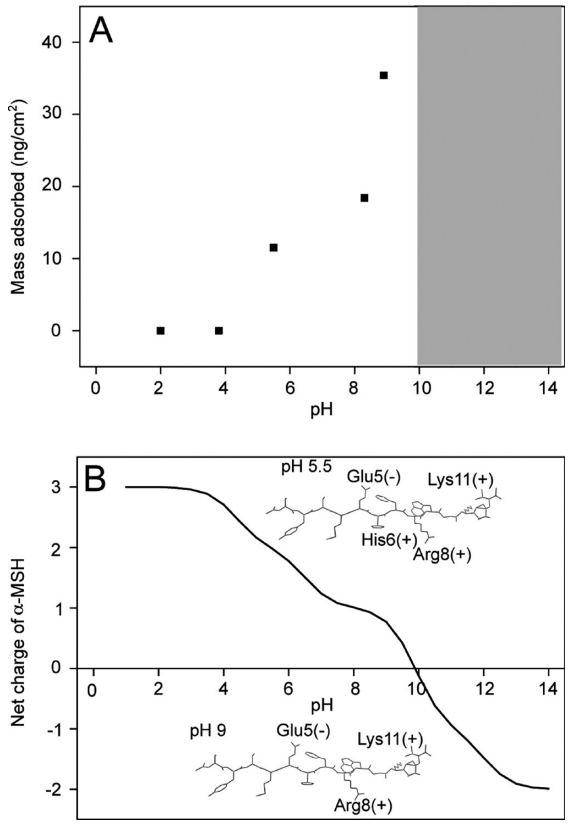

Figure 2. (A) Adsorption of α-MSH on a PLGA film from a 50 μg/mL solution as a function of pH as determined by QCM at 23.5 °C. Etching of PLGA surface occurs for pH values corresponding to the shaded region. (B) Net charge of α-MSH as a function of pH. The graphical insets show the key residues of α-MSH involved during surface adsorption at pH 9 and 5.5.

α-MSH,[16,17] confirming the dependence of multilayer assembly on these molecular properties.

3.2. Adsorption of α-MSH on PLGA Film. Hydrophobicity is another chemical property that can be exploited for the delivery of α-MSH as a means to build up layered materials to control peptide release. We have previously reported that α-MSH can be successfully adsorbed on a PLGA film at pH 5.5, most likely as a result of hydrophobic interactions between the polymer and peptide.[21] The adsorption of α-MSH on PLGA was examined as a function of pH to further explore and optimize this interaction with the intention of later constructing layers on top of this α-MSH layer.

The highest adsorption of α-MSH occurred at pH 9 close to the isoelectric point (pI) of 10, as illustrated in Figure 2. It is generally observed that maximum adsorption occurs in the isoelectric point region of the protein.[42] Steric repulsion within and between the α-MSH peptides is lowest close to the pI where the peptide has no net charge,[43] whereas the positive or negative charge at pH values lower or higher than the pI is likely to reduce peptide adsorption.

A rise in frequency was observed at pH 11, indicating a decrease in polymer mass (data not shown) that can be attributed to accelerated polymer etching and hydrolysis of the polymer backbone. This degradation occurs at solution pH of 10 or above[44] and it prevented measurements of α-MSH adsorption at pH values greater than 9. A solution of pH 9 is therefore optimal, limiting the charge on the α-MSH peptide and maximizing peptide adsorption while also avoiding significant degradation of the PLGA layer during adsorption.

Table 1. Secondary Structure of α-MSH in Various Buffers or after Adsorption and Release from a PLGA Surface into a Solution at near Physiological pH[a]

	α-helix	β-strand	turn	unordered structure
prior to loading				
in 10 mM Tris, pH 9	0.0	0.3	0.2	0.5
in 10 mM MES, pH 5.5	0.0	0.3	0.2	0.5
in water, pH 7	0.0	0.3	0.2	0.4
after loading at pH 9				
released in water, pH 7	0.0	0.4	0.2	0.4

[a] The proportion of secondary structures was estimated from the deconvolution of CD spectra using the DICHROWEB online server and CDSSTR algorithm.[27,28] Note fractions are rounded estimates and so may not sum to 1.0.

Two solution conditions of pH 9 and pH 5.5 were selected for all further experiments on α-MSH adsorption, as these represent the optimal conditions for adsorption of α-MSH and the HA and CS polyelectrolyte layers respectively. The expected distribution of charges on α-MSH at these pH values is shown in Figure 2.

3.3. Secondary Structure of α-MSH. The secondary structure of α-MSH was probed by far-UV circular dichroism (CD) to assess whether the peptide structure is altered by solution pH or on adsorption to a PLGA surface at the optimal pH of 9. The peptide had a predominantly random coil conformation at various solution pH values, with a similar proportion of β-strand and turn structure as determined by deconvolution of the CD spectra (Table 1). The shape of the spectra, shown in the Figure S2 in the Supporting Information, is consistent with our previous findings in water at pH 7 and observations made in the literature.[21,45] The peptide structure was also largely unchanged after adsorption at pH 9 and desorption near physiological pH (pH 7) from a PLGA surface (Table 1 and Figure S2), consistent with peptide behavior observed at pH 7.[21]

FTIR microscopy confirmed the presence of α-MSH with a predominantly disordered structure adsorbed on a PLGA surface at pH 9, as indicated by the peak at ~1670 cm^{-1} in the amide I region (Figure S3 in the Supporting Information). This finding is consistent with the CD data presented in Table 1. Taken together, these structural data indicate that the adsorption of α-MSH at pH 9 does not appear to adversely affect peptide structure, which is predominantly disordered and that these conditions may be used for the optimum loading of α-MSH in subsequent experiments.

3.4. Molecular Dynamics (MD) Simulations of α-MSH in Solution. We have performed complementary MD simulations of the α-MSH peptide at pH 9 and 5.5 to better understand the peptide behavior observed in solution by CD above. Six independent simulations were performed using different initial peptide conformations and trajectories of 600 ns were obtained for each simulation (Figure S1 in the Supporting Information). Unless otherwise stated, all quantitative results presented with regard to MD simulations are given as averages over the six independent trajectories for each system, with the first 50 ns of each trajectory excluded in order to reduce initial-structure-dependent bias. Uncertainties are expressed as standard errors of the means.

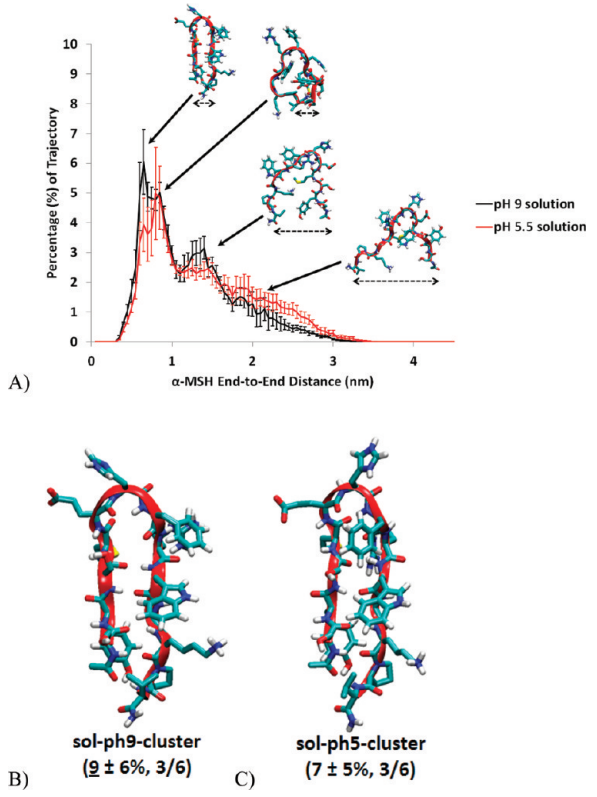

Figure 3. (A) Histograms of end-to-end (EE) distances (nm) for the combined trajectories of α-MSH in solution at pH 9 and 5.5. Error bars indicate standard errors of the means. Representative structures at selected EE distances are shown as insets, with dashed double-headed arrows illustrating EE distances. (B,C) Most highly populated conformation in solution at pH 9 (B) and 5.5 (C). Numbers in parentheses indicate average percentage of time structures exist within a trajectory (underlined) and uncertainties are expressed as standard errors. Fractions indicate the number of independent trajectories (out of 6) which exhibit the respective conformations.

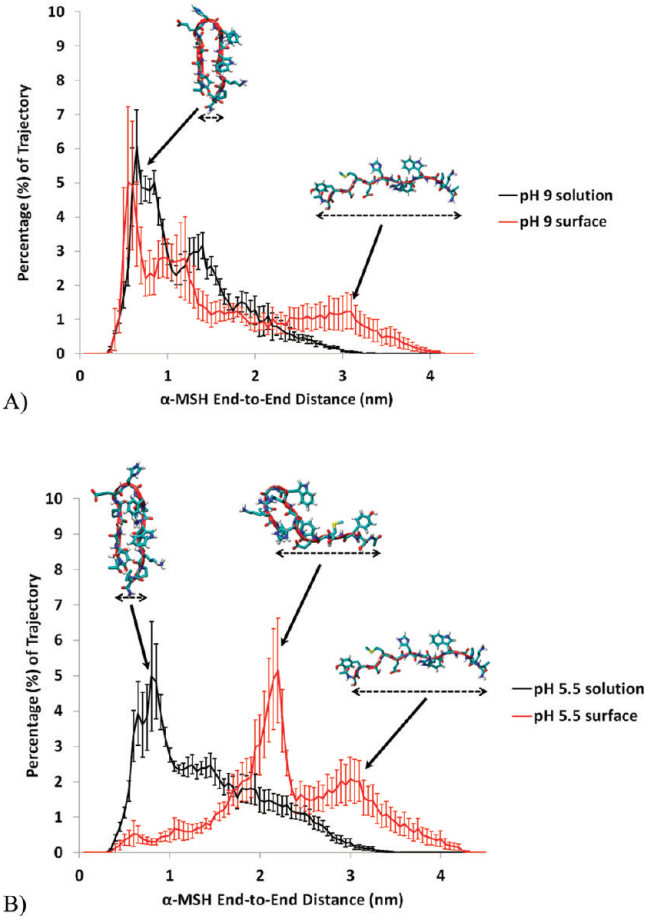

Figure 4. Histograms of EE distances (nm) for α-MSH in solution vs surface-adsorbed at (A) pH 9 and (B) at pH 5.5. Error bars indicate standard errors of the mean. Representative structures are inset.

Simulations of α-MSH in solution enable us to obtain insights into the structure and dynamics of the peptide at different pH, prior to interactions with surfaces. We note that, at both pH 9 and 5.5, the peptide exhibits substantial structural flexibility, exhibiting little secondary structure and adopts primarily disordered random coil structures, consistent with experimental data obtained by CD. This is evidenced by the rapid unraveling of the initial ideal α-helix for trajectories h-sol-ph9/5 and rapid collapse of the extended strand in x-sol-ph9/5 (see Table S1 in the Supporting Information for details of trajectory labels).

We have characterized the peptide structure with respect to its end-to-end (EE) distance, which is measured between the centers-of-mass of the N-terminal acetyl and C-terminal amide groups. Histograms for the combined trajectories at both pH values are shown in Figure 3A. Compact hairpin structures with EE distances <1 nm are preferred at both pH values, as indicated by the presence of sharp peaks ($\sim$5 $\pm$ 1%) in this region of the histograms. Despite this conformational preference, the peptide is also capable of adopting a relatively broad range of EE separations, indicative of its high flexibility at both pH values. Some differences are apparent, however, in the peptide conformation at the two pH values. There is a marginally greater preference for very compact structures (EE $\sim$ 0.7 and $\sim$1.2 nm) at pH 9 compared to pH 5.5. The higher population of compact structures at pH 9 is suggestive of somewhat greater structural rigidity at this pH. In contrast, the populations of more extended structures (EE > 1.5 nm) are higher at pH 5.5.

For each pH, we have clustered together structures with backbone root-mean-square deviation (rmsd) < 0.8 Å in order to determine the dominant peptide conformations and their relative populations, providing a measure of how often these structures appear during a simulation. These structures are shown in Figure 3B (pH 9) and Figure 3C (pH 5.5). At pH 9, the most dominant conformation (sol-ph9-cluster) was, on average, adopted 9 $\pm$ 6% of the time in each simulation trajectory. Its structure consists of a well-ordered β-hairpin, with a turn located at His[6]. The next most populated cluster was adopted 7 $\pm$ 3% of the time and likewise consists of a β-hairpin (data not shown). Other conformations were poorly populated (<4%), consisting largely of collapsed random coils. At pH 5.5, the dominant conformation (sol-ph5-cluster) was adopted on average 7 $\pm$ 5% of the time, again consisting of a β-hairpin, similar to that of sol-ph9-cluster. The remaining conformation clusters showed low population values (<4%) and consist of disordered hairpin structures.

Thus, at both pH values, the dominant conformation is a β-hairpin, although the majority of the conformations (>90%) are disordered. This is consistent with the secondary structure

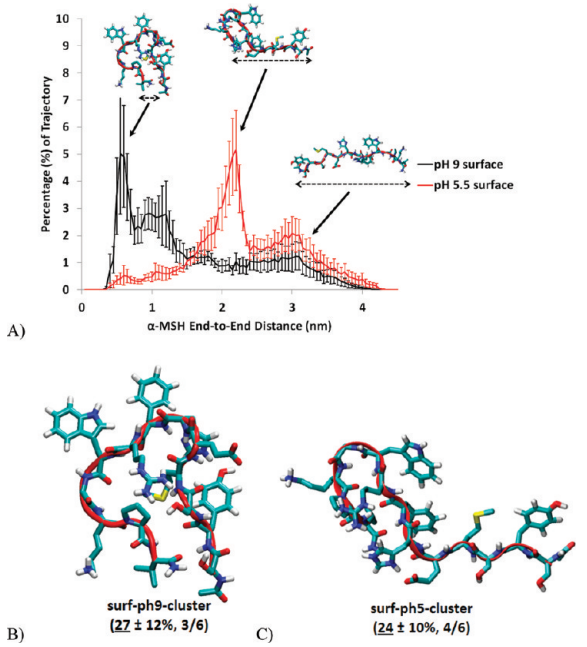

Figure 5. (A) Histogram of EE distances (nm) for α-MSH adsorbed onto surface at pH 9 and pH 5.5. Representative structures are inset. Error bars indicate standard errors of the mean. (B,C) Most highly populated conformations after surface adsorption at pH 9 (B) and 5.5 (C). Numbers in parentheses indicate average percentage of time structures exist within a trajectory (underlined) and uncertainties are expressed as standard errors. Fractions indicate the number of independent trajectories (out of 6) which exhibit the respective conformations.

determined by CD, which confirms the presence of β-strand, random coil and turn elements at both pH values (Table 1). The higher percentage of the dominant cluster at pH 9 (9%) compared to pH 5.5 (7%) suggests that the peptide is only marginally more structurally rigid at the former pH, consistent with the conclusions reached from inspection of the histograms of Figure 3A.

Overall, in solution, α-MSH exhibits similar structure and dynamics at pH 9 and 5.5.

3.5. MD Simulations of α-MSH on a Hydrophobic Surface. We have employed MD to acquire further insights into the molecular-level behavior of α-MSH on a PLGA surface, as observed experimentally by QCM and FTIR above. These insights are important for understanding the optimal presentation of α-MSH that will enable the development of a layered material for α-MSH delivery. Six independent simulations were performed, as above, using different initial peptide conformations and a model hydrophobic surface.

The gross effects on α-MSH structure and dynamics upon adsorption to a hydrophobic surface may be characterized by comparison of the histograms of EE distance for the peptide monomer in solution and after surface adsorption. This is shown in Figure 4A (pH 9) and Figure 4B (pH 5.5). These histograms indicate a substantial increase in the number of extended conformations upon adsorption at both pH values. In particular, fully extended structures, with end-to-end distances of >3 nm, appear as a result of surface adsorption; such highly extended structures are negligible in solution, as can be seen in Figure 4. There is also a concurrent and significant reduction in the populations of compact structures with EE distance between 0.5 and 1.7 nm.

At pH 9, there remains a strong preference for compact conformations after adsorption (EE distance ~0.7 nm; ~5 ± 2%). Thus, the "surface" histogram exhibits qualitatively similar features to that of the "solution" histogram (Figure 4A). In stark contrast, at pH 5.5 (Figure 4B), the equilibrium shifts substantially upon adsorption, with the peptide preferentially adopting extended structures with EE distance ~2.2 nm (5 ± 1%), rather than the far more compact hairpin structure that is preferred in solution (~0.7 nm).

pH-dependent differences in adsorption-induced peptide structural changes may be further elucidated by direct comparison of the EE distance histograms and conformation clusters for the surface-adsorbed systems at the two pH values studied. EE distance histograms for adsorbed peptide at pH 5.5 and 9 are shown in Figure 5A. Inspection of the two histograms indicates significant pH-dependent differences in conformational populations. In particular, at pH 9, α-MSH exhibits a bias toward compact structures, as indicated by the peaks at ~0.7 and 1.1 nm (5 ± 1% and 3 ± 0.5%, respectively). In contrast, at pH 5.5, the adsorbed peptide strongly favors more extended conformations, as indicated by the peaks at ~2.2 and 3 nm (5 ± 2% and 2 ± 0.5%, respectively). The presence of distinct peaks in the two histograms indicates that the peptide favors certain, discrete states, transitioning between them throughout the trajectories. The pH 9 histogram exhibits somewhat narrower peaks, which suggests marginally greater structural rigidity at this pH. This was also observed for the peptide in solution, as discussed above.

Cluster analysis sheds further light on the dominant surface-adsorbed structures at different pH values. At pH 9, the primary cluster (surf-ph9-cluster) appears, on average, 27 ± 12% of the time in the trajectories (Figure 5B). This cluster consists of a compact, disordered hairpin, with limited β-strand content. The remaining clusters have populations of <12% and likewise possess limited secondary structure content. At pH 5.5, the cluster with the highest population appears, on average, 24 ± 10% of the time, (surf-ph5-cluster; Figure 5C). This structure is elongated and consists of an extended segment composed of residues Ser^{1} to Trp^{9}, with a tight turn at Gly^{10} which facilitates hydrogen bonding between the polypeptide backbones of Lys^{11}-Val^{13} with those of Phe^{7}-Trp^{9}. The remaining clusters have populations of <4.5% and consist of disordered extended strands (data not shown). On the surface, in contrast to the peptide in solution, no significant β-hairpin structure was formed at either pH. Additionally, the formation of slightly more highly populated states at pH 9 (27%) compared to pH 5.5 (24%) indicates a marginally greater motional rigidity for the former, consistent with the narrower peaks in the pH 9 EE distance histogram (Figure 5A).

The marked difference between the major conformations of surface-adsorbed α-MSH at the two pH values studied may have important implications for the interaction between the peptide and hydrophobic surfaces, as well as the subsequent adsorption of molecules during LbL assembly in the development of multilayered materials. First, at pH 9, the peptide retains structural compactness upon adsorption to the surface (with an average radius of gyration R_g = 0.85 ± 0.04 nm), whereas at pH 5.5, the peptide strongly favors extended conformations (R_g = 0.96 ± 0.04 nm). Thus, at pH 5.5, each peptide "sweeps out" a larger area on the surface, increasing its effective size, thereby reducing the total number of peptides that may be adsorbed as a monolayer compared to the compact conformations favored at pH 9 which enable more peptides to be adsorbed as a monolayer. This may

partially explain the higher peptide loading at pH 9, as indicated by QCM data collected as a function of pH (Figure 2). Second, the marginally greater structural rigidity of the peptide at pH 9 may result in a higher uniformity of conformations, resulting in the stable presentation of residues (especially basic residues), which may interact favorably with any subsequent layering molecules, thereby facilitating multilayer film deposition. At pH 5.5, the peptide undergoes somewhat more structural fluctuations, which may render it more difficult for layering molecules to "seek out" and interact with peptides that already exist in a conformation most amenable to binding. Third, it is possible that the conformation of the peptide itself may influence the effectiveness with which it enables the subsequent adsorption of layering molecules. This is explored further below (3.6 layer-by-layer assembly).

To lend further insights into the residue-specific manner in which α-MSH interacts with a model hydrophobic surface and to explain why adsorption results in more extended conformations, we examined bar charts of the average number of contacts between each residue and particles of the hydrophobic surface within 4.5 Å at both solution pH values (Figure 6A). Qualitatively similar contact profiles are obtained for both pH 9 and 5.5. There are generally low numbers of contacts between the surface and hydrophilic or small hydrophobic residues (Ser, Met, Pro, Gly, and Val). The most significant contacts are formed with the aromatic residues Tyr, His, Phe, and Trp. This can be seen by visualization of the trajectories, which indicate that aromatic side chains form close contacts with the surface persistently for all surface-adsorption systems studied. An example is shown in Figure 6, C and D. All of the charged side chains form a relatively low number of surface contacts. Interestingly, despite its charge, Lys^{11} makes contacts with the nonpolar surface via the hydrocarbon portion of its side chain (Figure 6C). Thus, it is partially shielded by the surface and may not fully participate in further interactions with switching layer molecules. On the other hand, Arg^{8} forms negligible contacts with the surface and is instead fully solvated, pointing distal to the surface plane (Figure 6C). Additionally, Arg^{8} exhibits the highest solvent-accessible surface area (Figure 6B). Thus, Arg^{8} is available to form further interactions and may be more important than Lys^{11} for initial binding of negatively charged functional groups of the subsequent layering molecules.

The main difference in surface contact profiles between the two pH values studied is the markedly lower number of surface contacts with His^{6} at pH 5.5, which is charged at this pH (asterisked in Figure 6A). The loss of contacts with the (triply protonated) His^{6} could play a partial role in the lower adsorptive loading α-MSH on hydrophobic surfaces (such as PLGA) at pH 5.5 (Figure 2). We note that, with both positively and negatively charged surfaces, the peptide shows negligible contacts with the surface except for Arg (on negative surfaces) or Glu (on positive surfaces) (data not shown). This is consistent with the lack of binding of α-MSH on HA and CS as determined by QCM (Figure 1).

One limitation of our simulations as models of α-MSH/PLGA binding is the neglect of polar glycolide ester groups, which are expected to be present at the surface. Although the 75:25 PLGA surface employed in our current experiments (see section 2.1.1) is likely to consist largely of the (nonpolar) lactide, with peptide−surface binding therefore dominated by hydrophobic interactions, a relatively low fraction of peptides bound to the polar surface regions may still contribute to the LbL process. Peptide binding behavior at hydrophilic regions may also be

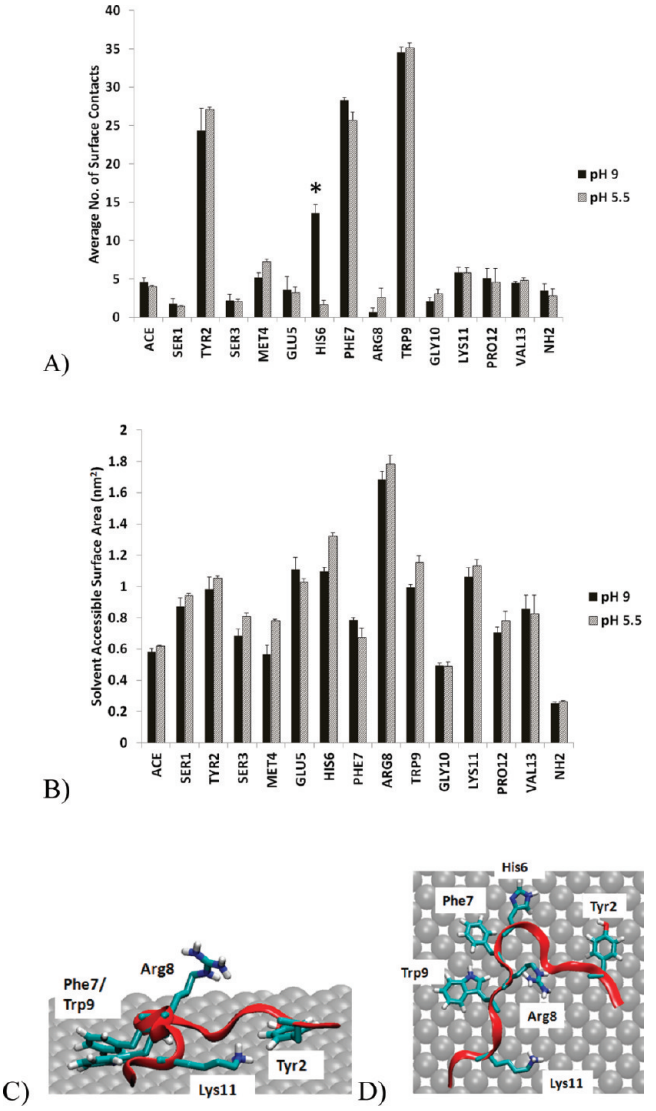

Figure 6. (A) Bar chart of average number of contacts between each residue (x-axis) and surface atoms, with error bars indicating standard errors over the trajectory-averaged values obtained for the six independent simulations at pH 9 and 5.5. (B) Bar chart of average solvent-accessible surface area (SASA) for each residue after surface-adsorption. (C) Graphical illustration of typical surface-adsorbed conformation at pH 9, viewed from elevation along a diagonal with respect to the surface plane and (D) viewed along the surface normal, with side chains of interest shown in liquorice form and labeled.

markedly different from that at the hydrophobic regions. Such differences are due to the specific, anisotropic nature of polar interactions (e.g., hydrogen bonds, which exhibit strong directionality), as opposed to the isotropic, nonspecific nature of hydrophobic interactions.

Several differences are possible for polar regions. α-MSH may be less laterally mobile upon binding to polar surface regions. Reduction in lateral motion has been demonstrated in simulation studies by Serr et al.,[46] who showed that the forced motion of a peptide on a polar surface exhibits "stick−slip" behavior, whereby the peptide shifts positions on the surface in a discrete, stepwise fashion, due to the breaking and re-formation of hydrogen bonds. In contrast, motion on a hydrophobic surface was shown to be smoother. There are also likely to be differences in peptide

conformation and internal dynamics. Roach et al. observed that proteins exhibit greater secondary structure upon adsorption to a polar surface compared to a hydrophobic surface,[47] an effect also examined computationally.[48] We therefore speculate that α-MSH may retain more β-strand content upon adsorption to a polar surface, with more narrow peaks in the EE distance histograms. It is also likely that different residues (especially polar and charged residues) of α-MSH will bind to a polar surface, compared to a nonpolar surface, thus exposing different groups for subsequent interaction with LbL layering molecules. In particular, while His^6 makes few contacts with a hydrophobic surface at pH 5.5 owing to its charge, it is expected to enable the peptide to bind more strongly to a polar surface at this pH. The fraction of α-MSH that binds to polar surface regions is expected to be small, however, since there is only 25% of the surface that is affected based on the PLGA monomer ratio (75:25) used in this study. The lower loading of α-MSH at pH 5.5 compared to pH 9 (discussed in section 3.2 above) suggests that the peptide primarily adsorbs at hydrophobic regions of the PLGA surface, with the glycolide ester groups playing a relatively minor role.

While the development of a surface that more faithfully represents amorphous PLGA is worthy of further study, our model surface does provide valuable insight into the behavior of α-MSH for this system. First, as mentioned above, the PLGA films and microspheres used in the present work consist of lactide:glycolide in a 75:25 ratio. Thus, the PLGA surface is likely to consist largely of the (hydrophobic) lactide. There is also evidence for the segregation and enrichment of $-CH_3$ groups at thin-film PLGA surfaces prepared via solvent casting, as discussed by Paragkumar et al., although this effect is attenuated by surface wetting.[49] This behavior is expected to apply in the 2D PLGA films used in the QCM studies here but may deviate in the PLGA microspheres produced using the emulsion technique. The microspheres possess a slightly negative ζ potential due to the residual PVA, although this is expected to be lower in the PLGA films prepared using the solvent casting method for the QCM experiment.[50] In addition, the well-documented problem of nonspecific protein binding to PLGA suggests that the interaction is primarily hydrophobic (e.g., between exposed core residues and the surface);[51,52] indeed, we have also previously shown that α-MSH adsorbs on a PLGA film at pH 5.5, most likely as a result of hydrophobic interactions.[21] Therefore, the primary mode of binding between proteins/peptides and PLGA is likely to involve nonspecific, hydrophobic interactions, which are captured well by our model.

3.6. Layer-by-Layer Assembly. The ability of α-MSH to act as a building block and initial layer for the construction of a layer-by-layer material including HA and CS molecules was assessed using α-MSH-coated PLGA films. The α-MSH peptide was adsorbed from solution at pH 9 or pH 5.5 to test the hypothesis that the greater mass of α-MSH observed by QCM at pH 9 and more favorable orientation predicted by MD simulation for this condition would enable the successful deposition of layers compared to at pH 5.5.

Both electrostatic and hydrophobic interactions were explored as a means to introduce the subsequent layer on top of the α-MSH coated surface, described here as the switching layer, due to its role in switching the assembly to HA and CS polyelectrolyte layers. Three switching layers were selected: zwitterionic lipid DOPC, negatively charged lipid mixture DOPC/DOPS at a ratio of 4:1, and negatively charged linear polysaccharide HA. The ratio in the DOPC/DOPS preparation was selected based on its ability to form stable supported lipid bilayers on various surfaces such as silica.[53,54] The chemical structures of the three-component biomolecules are shown in Figure 7.

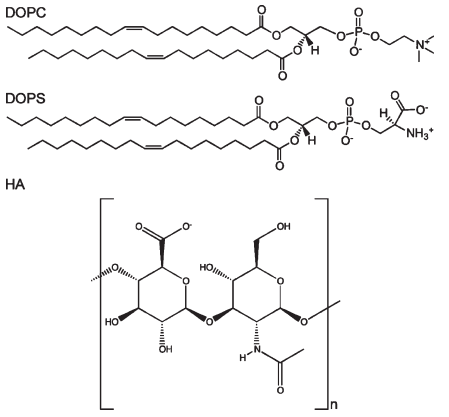

Figure 7. Chemical structures of DOPC, DOPS, and HA used as switching layers in the multilayer assemblies constructed on top of the α-MSH-coated PLGA surfaces.

The lipid switching layers were selected to interact with the hydrophobic residues (Met^4, Phe^7, Val^{13}) of the α-MSH peptide. The charged headgroup on the DOPC/DOPS mixture may also enable subsequent layering with HA and CS molecules. The chain length of each of the two lipids (18 carbon alkane chains with a double bond at the ninth carbon position) was selected such that the lipids have similar hydrophobicity. In contrast, HA is a weak polyanion with one carboxylic acid group per disaccharide unit at pH 9 and 5.5, selected to exploit possible interactions with the positively charged residues in α-MSH (Arg^8, Lys^{11}), which give rise to a net charge of +1 and +2 at pH 9 and 5.5, respectively. Positively charged CS was not studied due to the like charges on the CS and α-MSH molecules, which are expected to inhibit interactions and prevent the formation of a stable layer.

Multilayers were successfully constructed using all three switching layers following the adsorption of an α-MSH layer at pH 9, as shown in Figure 8, where the mass of α-MSH adsorbed (70 ± 30 ng/cm^2) is similar to that observed under the same conditions in Figure 2. All overtones measured showed similar trends and consequently only changes in the frequency and dissipation for the third overtone are shown. These results show that short peptides such as α-MSH can be used as the base building block for the construction of layered assemblies. The mass of the switching layer deposited immediately after the α-MSH layer differed for the three switching preparations (Figure 8B−D). The rate of HA and CS layer growth was also different between treatments but was relatively linear in each case, similar to reports of HA-CS multilayers on a PLGA film under conditions close to those used here.[23]

The negatively charged lipid DOPC/DOPS mixture gave rise to the highest mass deposition in the switching layer (Figure 8B) with a frequency change of 13 ± 5 Hz, corresponding to 0.3 ± 0.1 nmol/cm^2 (240 ± 90 ng/cm^2) of lipid when adsorbed at pH 5.5. The overall layer mass was also greatest (4030 ± 270 ng/cm^2), due to a greater mass of HA and CS layers. A pH of 5.5 was selected for deposition of the switching layer, as the phosphoserine head groups on DOPS have a net negative charge of −1 under these conditions; this pH is also optimal for deposition of subsequent HA and CS layers.

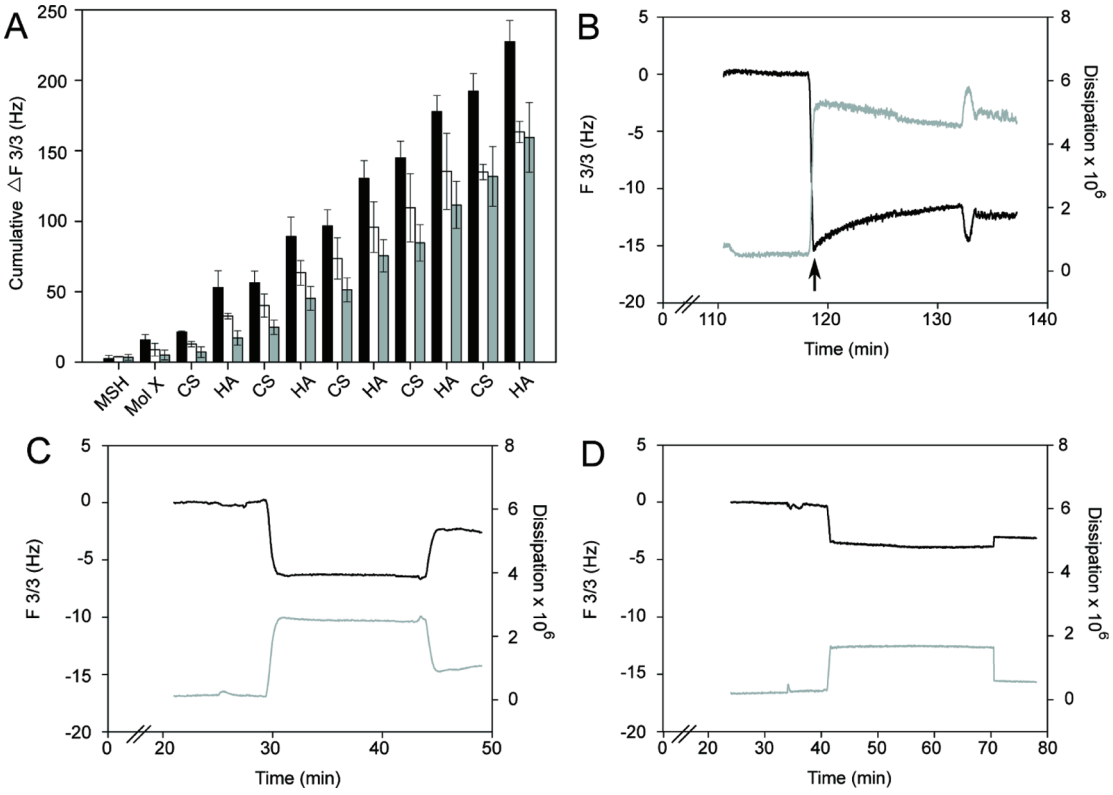

Figure 8. (A) Changes in the cumulative frequency at the third overtone showing the multilayer assembly of lipid, HA, and CS on an α-MSH-coated PLGA film as determined by QCM. The α-MSH peptide was adsorbed at pH 9. Molecule X refers to the switching layers of DOPC/DOPS mixture (black), HA (white), or DOPC (gray). DOPC was adsorbed at pH 9 whereas HA or the DOPC/DOPS mixture were adsorbed at pH 5.5. All subsequent layers were assembled at pH 5.5. Each data point is the mean $\pm$ s.d (n = 4 for DOPC/DOPS, n = 3 for HA, and n = 6 for DOPC). (B,D) Changes in the frequency (black line) and dissipation (gray line) at the third overtone showing the deposition of (B) DOPC/DOPS, (C) HA, and (D) DOPC on an α-MSH-coated surface as measured by QCM. Liposome breakage is indicated by the arrow.

The high adsorption after the DOPC/DOPS layer could result from greater charge interactions between the positively charged α-MSH layer and the negatively charged lipid headgroups of the DOPS, compared to the other switching layers. This finding is in agreement with a previous study reporting favorable interactions between α-MSH and the negatively charged lipid DMPG (1,2-dimyristoyl-*sn*-glycero-3-phosphoglycerol).[45] An alternate explanation is that the DOPC/DOPS mixture forms a bilayer. Figure 8B shows that, upon liposome addition, the frequency decreases almost instantly which indicates that the liposomes bind to the surface. This was then immediately followed by an increase in the frequency and a corresponding decrease in the dissipation (shown by the arrow in Figure 8B). This phenomenon can be attributed to the breakup of the liposomes into a bilayer, resulting in the loss of water previously contained within the liposomes.[55] Interactions between the peptide and lipids may be further stabilized by DOPC/DOPS bilayer formation, as it has been reported previously that α-MSH associated well with 2-dimyristoyl-*sn*-glycero-3-phosphoglycerol (DMPG) lipid bilayers and this could further facilitate layering.[45]

The use of HA as a switching molecule resulted in less mass deposition compared to the DOPC/DOPS mixture, with a cumulative change in frequency of 5 $\pm$ 4 Hz (90 $\pm$ 80 ng/cm^2) when adsorbed after the α-MSH layer at pH 5.5, as shown in Figure 8C. The relatively high standard deviation could be due to the small amount of material being deposited, which gives rise to a large variability. The growth of the subsequent HA and CS layers was initially similar to that observed for DOPC/DOPS but the final mass after 10 layers was significantly less (2890 $\pm$ 140 ng/cm^2). Polyelectrolytes are reported to anchor well on surfaces coated with protein, as the patched nature of charge presented by the protein surface is thought to allow linear polyions to penetrate between protein molecules, optimizing electrostatic interactions.[56] HA, however, is a relatively weak polyion. α-MSH is also short with only three charged residues at pH 5.5. These two factors are likely to limit the number of contact points between HA and the small peptide and restrict the subsequent growth of layers compared to DOPC/DOPS.

The adsorption of zwitterionic DOPC after α-MSH resulted in a cumulative change in frequency of 2 $\pm$ 1 Hz (0.05 $\pm$ 0.03 nmol/cm or 40 $\pm$ 20 ng/cm^2), the least observed for all three switching layers, as shown in Figure 8D. The zwitterionic DOPC lipid presents a phosphocholine headgroup with a net charge of 0 at both pH 9 and pH 5.5, as a result of the positively charged phosphate group and negatively charged terminal choline group. DOPC adsorption was therefore carried out at pH 9, rather than at pH 5.5 as used for the other two switching molecules, to minimize the charge on α-MSH and maximize hydrophobic interactions between the peptide and the DOPC lipid preparation.

The successful buildup of multilayers after DOPC adsorption indicates that hydrophobic interactions can be used to build multilayers on top of a layer of small peptides. The effectiveness of this mechanism seems similar to that of electrostatic

interactions with HA with a total mass of 2820 ± 440 ng/cm^2 after 10 layers. The hydrophobic mechanism is, however, significantly less effective than that of the negatively charged and hydrophobic lipid mixture DOPC/DOPS. Preliminary experiments showed that DOPC binds strongly to an unmodified PLGA surface with a frequency change of 30 ± 3 Hz (Figure S4 in the Supporting Information). The much smaller change in frequency due to adsorption of DOPC on an α-MSH-coated PLGA film thus suggests that there is minimal interaction between the peptide and DOPC. This result is consistent with the literature, where NMR has been reported to show minimal interactions between α-MSH and neutral lipids compared to negatively charged lipids.[57]

The multilayers constructed here on top of all three switching layers can potentially be improved by increasing the salt concentration, which has been shown to shield charges on polyelectrolytes. This can allow a coiled structure and higher charge overcompensation for the HA and CS molecules, leading to a greater deposition of mass within polyelectrolyte layers.[58,59]

It is notable that the strong hydrophobic interaction between α-MSH and the PLGA surface, also observed in the MD simulations, prevented desorption of the α-MSH peptide when the buffer was changed from a pH of 9 to 5.5 prior to adsorption of DOPC/DOPS or HA layers (data not shown). The multilayer films fabricated here with each of the three switching layers were also stable when the pH was alternately changed from 5.5 to physiological pH (pH 7.4) in a pH challenge following the construction of layers (data not shown). Under these conditions, the films swell and contract with no apparent loss in mass. This is due to the addition of cross-linkers at each step of HA deposition, which is known to link the alternate layers.[23]

The adsorption of α-MSH on PLGA from a solution at pH 5.5 was also studied by QCM, as shown in Figure 9. The adsorption of α-MSH was ~30 ± 8 ng/cm^2 under these conditions, which is approximately 2.5-fold lower than at pH 9, consistent with the data presented in Figure 2. The mass of DOPC/DOPS switching layer was also significantly less than at pH 9 with 0.02 ± 0.02 nmol/cm^2 (20 ± 14 ng/cm^2) deposited. There was no evidence of bilayer formation by DOPC/DOPS under these conditions, consistent with the lower mass of lipid. The reduced DOPC/DOPS layer resulted in a significantly lower mass in subsequent polyelectrolyte layers with a total mass of 200 ± 180 ng/cm^2 adsorbed four layers after the addition of α-MSH compared to 1000 ± 150 ng/cm^2 adsorbed after the addition of α-MSH at pH 9.

While the mass of HA or DOPC switching layers deposited at pH 5.5 and subsequent polyelectrolyte layers was within the variation observed for layer deposition at pH 9, it was clearly evident that the deposition of polyelectrolyte layers in all three assemblies studied at pH 5.5 was suboptimal, with HA desorbing immediately upon introduction to the QCM chamber, as illustrated in Figure 9B for the HA-based assembly. Frequency changes for the multilayer films formed using the other two switching layers (DOPC/DOPS and DOPC) are shown in Figure S5 in the Supporting Information. Layers could be established under these conditions with 20 ± 4 ng/cm^2 of HA or 0.10 ± 0.01 nmol/cm^2 (80 ± 9 ng/cm^2) of DOPC deposited, leading to a total mass of 380 ± 160 ng/cm^2 or 360 ± 130 ng/cm^2 after four layers but the arrangement of polyelectrolyte molecules and layering process appeared compromised compared to at pH 9.

The 2.5-fold reduced mass of α-MSH on the PLGA film at pH 5.5 compared to at pH 9 results in the 3 × 10^{13} fewer charges per cm^2 of surface, based on the charges shown in Figure 2. The

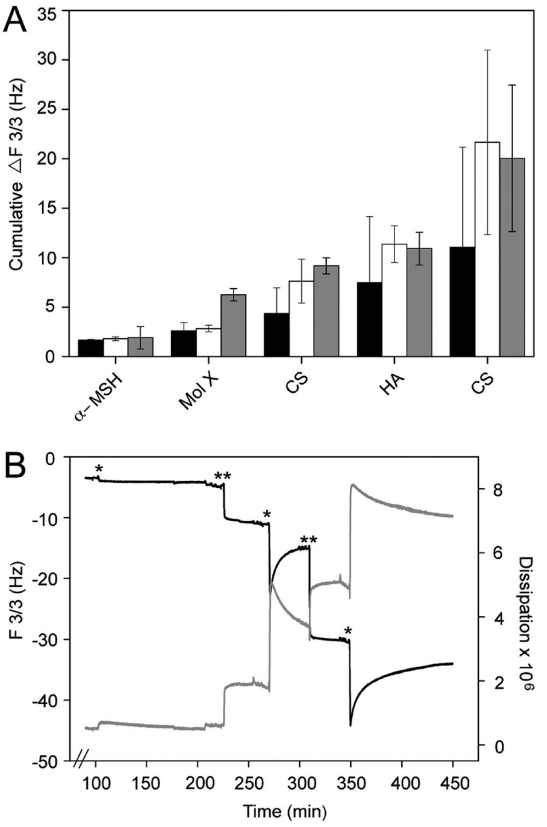

Figure 9. (A) Cumulative frequency changes at the third overtone during the multilayer assembly of lipid, HA, and CS on an α-MSH-coated PLGA film as determined by QCM. The α-MSH peptide was adsorbed at pH 5.5. Molecule X refers to the switching layer of DOPC/DOPS mixture (black), HA (white), or DOPC (gray). DOPC was adsorbed at pH 9 whereas HA or the DOPC/DOPS mixture were adsorbed at pH 5.5. All subsequent layers were adsorbed at pH 5.5. (B) Changes in the frequency (black line) and dissipation (gray line) at the third overtone showing the deposition of HA (*) and CS (**) when HA was used as the switching layer shown in (A), as measured by QCM.

MD simulations also indicate that the peptide has greater structural rigidity at pH 9, with a strong preference for compact disordered hairpin structures when adsorbed on a surface. The higher density of such structures may lead to a high surface capacity to absorb charged layering molecules, whereas the extended structures observed in the simulations at pH 5.5 may facilitate less binding of layering molecules. The compact structures at pH 9 also present Arg^8 toward the next layer, suggesting interactions with anionic layer molecules will be favorable. The reduced charge and altered arrangement of α-MSH adsorbed at pH 5.5 are likely responsible for the reduced stability for all assemblies and reduced layer mass for DOPC/DOPS. Given the strong preference for compact hairpin structures (predicted by MD) and the experimentally observed higher LbL efficacy at pH 9, we postulate that a cyclized form of α-MSH (which would lock the peptide in a tight hairpin conformation) may be more effective than the native linear form of the peptide in acting as a template in LbL assembly, particularly at pH 5.5.

It is important to take care when using cross-linking reagents in systems containing biomolecules so that their bioactivity is not adversely affected. It is expected that the presence of excess cross-linker during the addition of HA switching layer as used here will

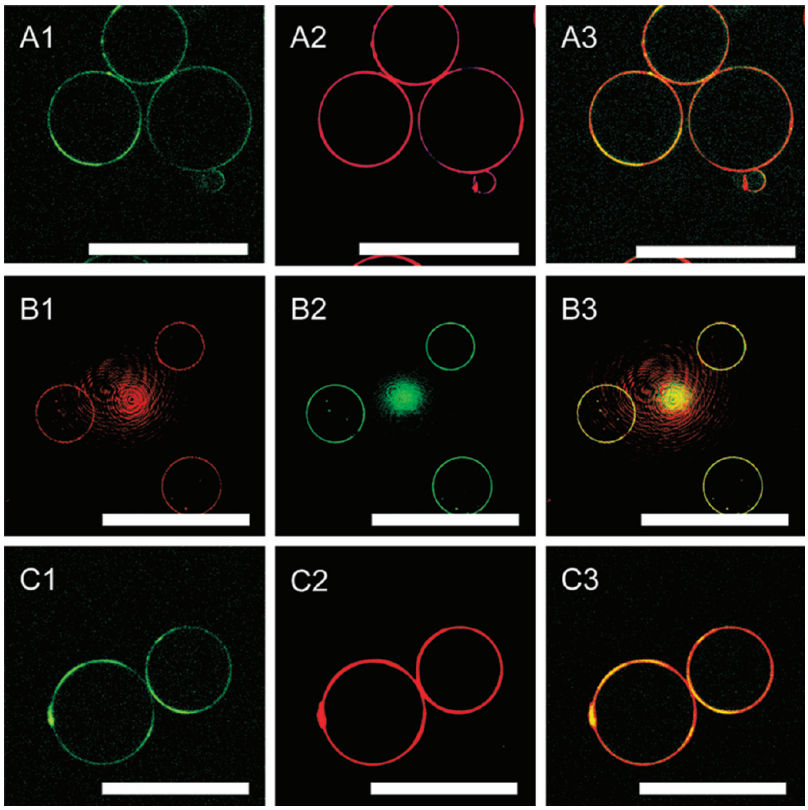

Figure 10. Confocal laser scanning microscopy images of multilayer coatings assembled on PLGA microspheres: (A) α-MSH-DOPC/DOPS$^{NBD\text{-}PC}$-(CS-HA)$_4$-CS^{Rhd}-HA; (B) α-MSH-HA-CS^{Rhd}-(HA-CS)$_3$-HA-CS^{AF488}-HA; and (C) α-MSH-DOPC$^{NBD\text{-}PC}$-(CS-HA)$_4$-CS^{Rhd}-HA. Column 1 shows the first fluorescently labeled molecule; lipid mixtures containing fluorescently labeled nitrobenzoxadiazole phosphocholine (lipid$^{NBD\text{-}PC}$) for treatment A and C or rhodamine-labeled chitosan (CS^{Rhd}) for treatment B. Column 2 shows the CS^{Rhd} for treatments A and C or the second chitosan which was fluorescently labeled with Alexa Fluor 488 (CS^{AF488}) for treatment B. Column 3 shows the composite images of columns 1 and 2. Adsorption of the α-MSH peptide was performed at pH 9. The scale bars are 50 μm in length in all images. The interference pattern in images B 1−3 is a scattering artifact from the top of a microsphere.

have minimal effect on the structure and bioactivity of α-MSH. EDC is highly unstable in aqueous solution and is quickly hydrolyzed.[60] Furthermore, α-MSH only has one available amine group which comes from the lysine residue at position 11 as the N-terminus of the peptide is acetylated. On the basis of the MD simulation, lysine is partially shielded from the surface as it makes contact with the PLGA surface through the hydrocarbon portion of its side chain (Figure 6C). This will minimize the possibility of α-MSH being cross-linked to HA. It is possible, however, that the excess cross-linker might activate the carboxyl group on the glutamic acid residue at position 5 to NHS-ester form. This NHS-ester is not expected to react with the amine group of CS due to the barrier provided by the switching layer of HA and the lipids. The potential effect of cross-linking on the bioactivity of the peptide will be explored in an upcoming study. A previous study using EDC and NHS as cross-linkers under the same conditions as those used here to sandwich basic fibroblast growth factor (bFGF) between multilayers of heparin, HA, and CS has shown that bFGF retained its bioactivity upon release.[7] This indicates that the conditions of the cross-linking technique employed here should have minimal adverse affects on the loaded biomolecules.

Successful LbL deposition is known to be facilitated by the overcompensation of charges, which in turn promotes the binding of the subsequent polyelectrolytes.[1] Previous studies suggest that for electrostatically driven LbL deposition of poly(sodium 4-styrenesulfonate) (PSS) and poly(diallyldimethylammonium chloride) (PDADMAC) - *N*-methyl-*N*-vinylacetamide (NMVA) copolymers with varying density, both the substrate and the polyelectrolyte species must be sufficiently charged. If the charge is insufficient, the adsorbed layers may be partially removed upon adsorption on the next polyelectrolyte layer,[61] similar to behavior observed here when the multilayers were assembled on α-MSH adsorbed at pH 5.5. The authors suggest that the behavior of PSS and PDADMAC is due to the formation of free polyelectrolyte complexes in solution, which are entropically favored compared to a multilayer on the surface,[62] and similar complexes may occur when α-MSH is adsorbed at pH 5.5.

Together, these experiments show that the mass, presentation, and charge of α-MSH adsorbed on a surface must be optimized to allow a subsequent LbL coating to be constructed. While both electrostatic and hydrophobic interactions can be used to drive LbL assembly, the combination of electrostatic and hydrophobic interactions is most successful for layer construction on top of this hydrophobic and charged short peptide.

3.7. Translation to a 3D Surface. The methods used to construct the three layer-by-layer assemblies on an α-MSH-coated surface deposited at pH 9 were successfully translated from a planar to 3D surface using PLGA microspheres, as shown by the confocal microscopy images in Figure 10. The lipid switching layers DOPC/DOPS or DOPC and the third layer of CS were fluorescently labeled as shown in Figure 10, A1, C1, and B1,

respectively. The fluorescence in these layers was relatively weak and uneven, indicating the slow growth of early layers and small mass deposition consistent with the QCM data in Figure 8. In contrast, relatively uniform and strong fluorescence was observed from the eleventh layer of labeled CS for all three treatments, as shown in Figure 10, A2, B2, and C2, consistent with stable film development over multiple layers. These images confirm the potential of such multilayers to act as capping layers to tune the release profile of α-MSH.

Further control could be introduced with multiple DOPC/DOPS lipid layers to utilize the association between the negatively charged lipid and α-MSH and/or PLGA layers. Deposition of multiple PLGA layers has been used to create multiple compartments within LbL constructs on a 2D surface consisting of layers that degrade slowly.[63] This method could be adapted to incorporate multiple layers of the α-MSH peptide on a 3D microsphere to increase the dose of this antiinflammatory peptide.

The multilayers formed in this study could also potentially be applied on nanoparticles with further optimization. One factor that may need to be altered to achieve this application is the molecular weight of the polyelectrolytes. The length of HA and CS used here may be too long for nanoparticles and may cause them to aggregate due to interactions between the polyelectolytes on different particles.[64]

4. CONCLUSION

We have shown that a short model hydrophobic peptide can be adsorbed near to its pI on a hydrophobic surface and used as the initial building block in the LbL assembly of biomolecules without modification of the peptide structure. The mass and orientation of the peptide on the surface were optimized when the solution was near to the pI of the peptide and these properties are shown to improve the formation of multilayers significantly. Molecular dynamics simulations provide insight into the structure of the peptide in solution and on a hydrophobic surface as a function of pH and allow a better understanding of how the peptide interacts with subsequent molecules, in this case lipids and linear polysaccharides. The multilayer constructs developed here can be potentially used as means to load therapeutics in the form of either small or large molecular weight drugs or peptides and may act as a capping layer to tune the therapeutic release profile. Molecular dynamics simulation offers great potential as a screening technique to determine the optimum structure and orientation of the adsorbed peptide or drug as a function of solution pH or surface chemistry, which in turn can be used to develop more robust layered assemblies.

■ ASSOCIATED CONTENT

Supporting Information. The starting conformations of the α-MSH used in the MD simulations are illustrated in Figure S1. Circular dichroism and Fourier transform infrared spectra of the peptide in solution and when adsorbed on PLGA microspheres are shown in Figures S2 and S3, respectively. QCM data showing the adsorption of zwitterionic lipid, DOPC, on PLGA surface is shown in Figure S4, QCM data showing multilayer deposition after α-MSH adsorption at pH 5.5 is in Figure S5. Table S1 summarizes the details of the MD simulations performed. This material is available free of charge via the Internet at http://pubs.acs.org.

■ AUTHOR INFORMATION

Corresponding Author
*E-mail: sgras@unimelb.edu.au.

■ ACKNOWLEDGMENT

The authors acknowledge the Particulate Fluids Processing Centre, a Special Research Centre of the Australian Research Council, for access to infrastructure. We also thank Dr. Brigitte Stadler and Miss Rona Chandrawati for their assistance in QCM, Dr. John Forsythe for QCM access and Dr. Mark Tobin and his team from the Infrared beamline at the Australian Synchrotron for assistance with the FTIR microscopy. We thank the National Computational Infrastructure (NCI), the Victorian Life Sciences Computation Initiative (VLSCI) and the Victorian Partnership for Advanced Computing (VPAC) for their generous provision of computational resources.

■ REFERENCES

(1) Decher, G. *Science* **1997**, *277*, 1232–1237.
(2) Lavalle, P.; Voegel, J. C.; Vautier, D.; Senger, B.; Schaaf, P.; Ball, V. *Adv. Mater.* **2011**, *23*, 1191–1221.
(3) Haynie, D. T.; Zhang, L.; Rudra, J. S.; Zhao, W. H.; Zhong, Y.; Palath, N. *Biomacromolecules* **2005**, *6*, 2895–2913.
(4) Becker, A. L.; Johnston, A. P. R; Caruso, F. *Small* **2010**, *6*, 1836–1852.
(5) Such, G. K.; Johnston, A. P. R; Caruso, F. *Chem. Soc. Rev.* **2011**, *40*, 19–29.
(6) Detzel, C. J.; Larkin, A. L.; Rajagopalan, P. *Tissue Eng. Part B—Rev.* **2011**, *17*, 101–113.
(7) Go, D. P.; Gras, S. L.; Mitra, D.; Nguyen, T. H.; Stevens, G. W.; Cooper-White, J. J.; O'Connor, A. J. *Biomacromolecules* **2011**, *12*, 1494–1503.
(8) Newman, D. J.; Cragg, G. M. *J. Nat. Prod.* **2007**, *70*, 461–477.
(9) Mart, R. J.; Osborne, R. D.; Stevens, M. M.; Ulijn, R. V. *Soft Matter* **2006**, *2*, 822–835.
(10) Song, W. X.; He, Q.; Mohwald, H.; Yang, Y.; Li, J. B. *J. Controlled Release* **2009**, *139*, 160–166.
(11) Wang, X. F.; Ji, J. *Langmuir* **2009**, *25*, 11664–11671.
(12) Benkirane-Jessel, N.; Lavalle, P.; Meyer, F.; Audouin, F.; Frisch, B.; Schaaf, P.; Ogier, J.; Decher, G.; Voegel, J. C. *Adv. Mater.* **2004**, *16*, 1507–1511.
(13) Hosta-Rigau, L.; Stadler, B.; Yan, Y.; Nice, E. C.; Heath, J. K.; Albericio, F.; Caruso, F. *Adv. Funct. Mater.* **2010**, *20*, 59–66.
(14) Kabanov, V. A.; Zezin, A. B. *Pure Appl. Chem.* **1984**, *56*, 343–354.
(15) Haynie, D. T.; Balkundi, S.; Palath, N.; Chakravarthula, K.; Dave, K. *Langmuir* **2004**, *20*, 4540–4547.
(16) Prouty, M.; Lu, Z. H.; Leuschner, C.; Lvov, Y. *J. Biomed. Nanotechnol.* **2007**, *3*, 184–189.
(17) Etienne, O.; Picart, C.; Taddei, C.; Haikel, Y.; Dimarcq, J. L.; Schaaf, P.; Voegel, J. C.; Ogier, J. A.; Egles, C. *Antimicrob. Agents Chemother.* **2004**, *48*, 3662–3669.
(18) Haynie, D. T.; Palath, N.; Liu, Y.; Li, B. Y.; Pargaonkar, N. *Langmuir* **2005**, *21*, 1136–1138.
(19) Schultz, P.; Vautier, D.; Richert, L.; Jessel, N.; Haikel, Y.; Schaaf, P.; Voegel, J. C.; Ogier, J.; Debry, C. *Biomaterials* **2005**, *26*, 2621–2630.
(20) Fioretti, F.; Mendoza-Palomares, C.; Helms, M.; Al Alam, D.; Richert, L.; Arntz, Y.; Rinckenbach, S.; Garnier, F.; Haikel, Y.; Gangloff, S. C.; Benkirane-Jessel, N. *ACS Nano* **2010**, *4*, 3277–3287.
(21) Go, D. P.; Palmer, J. A.; Gras, S. L.; O'Connor, A. J. *J. Biomed. Mater. Res., Part A* **2012**, *100A*, 507–517.
(22) Zhao, W. H.; Zheng, B.; Haynie, D. T. *Langmuir* **2006**, *22*, 6668–6675.

(23) Croll, T. I.; O'Connor, A. J.; Stevens, G. W.; Cooper-White, J. J. *Biomacromolecules* **2006**, *7*, 1610–1622.
(24) Stadler, B.; Chandrawati, R.; Goldie, K.; Caruso, F. *Langmuir* **2009**, *25*, 6725–6732.
(25) Marx, K. A. *Biomacromolecules* **2003**, *4*, 1099–1120.
(26) Thissen, H.; Chang, K. Y.; Tebb, T. A.; Tsai, W. B.; Glattauer, V.; Ramshaw, J. A. M.; Werkmeister, J. A. *J. Biomed. Mater. Res., Part A* **2006**, *77A*, 590–598.
(27) Whitmore, L.; Wallace, B. A. *Nucleic Acids Res.* **2004**, *32*, W668–W673.
(28) Compton, L. A.; Johnson, W. C. *Anal. Biochem.* **1986**, *155*, 155–167.
(29) Berendsen, H. J. C.; Postma, J. P. M.; van Gunsteren, W. F.; Hermans, J. In *Intermolecular Forces*; Pullman, B., Ed.; Reidel: Dordrecht, The Netherlands, 1981; p 331.
(30) Kwasigroch, J. M.; Rooman, M. *Bioinformatics* **2006**, *22*, 1800–1802.
(31) Berendsen, H. J. C.; Vanderspoel, D.; Vandrunen, R. *Comput. Phys. Commun.* **1995**, *91*, 43–56.
(32) Hess, B.; Bekker, H.; Berendsen, H. J. C.; Fraaije, J. *J. Comput. Chem.* **1997**, *18*, 1463–1472.
(33) Van der Spoel, D.; Lindahl, E.; Hess, B.; Groenhof, G.; Mark, A. E.; Berendsen, H. J. C. *J. Comput. Chem.* **2005**, *26*, 1701–1718.
(34) Lindahl, E.; Hess, B.; van der Spoel, D. *J. Mol. Model.* **2001**, *7*, 306–317.
(35) Gunsteren, W. F. V.; Billeter, S. R.; Eising, A. A.; Huenenberger, P. H.; Krueger, P.; Mark, A. E.; Scott, W. R. P.; Tironi, I. G. *Biomolecular simulation: The GROMOS96 manual and user guide*; Groninger: Zurich, 1996.
(36) Oostenbrink, C.; Soares, T. A.; van der Vegt, N. F. A.; van Gunsteren, W. F. *Eur. Biophys. J. Biophys.* **2005**, *34*, 273–284.
(37) Oostenbrink, C.; Villa, A.; Mark, A. E.; Van Gunsteren, W. F. *J. Comput. Chem.* **2004**, *25*, 1656–1676.
(38) Darden, T.; York, D.; Pedersen, L. *J. Chem. Phys.* **1993**, *98*, 10089–10092.
(39) Berendsen, H. J. C.; Postma, J. P. M; Vangunsteren, W. F.; Dinola, A.; Haak, J. R. *J. Chem. Phys.* **1984**, *81*, 3684–3690.
(40) Humphrey, W.; Dalke, A.; Schulten, K. *J. Mol. Graphics* **1996**, *14*, 33–38.
(41) Chuang, H. F.; Smith, R. C.; Hammond, P. T. *Biomacromolecules* **2008**, *9*, 1660–1668.
(42) Norde, W. *Adv. Colloid Interface Sci.* **1986**, *25*, 267–340.
(43) Tsai, T. M.; Mehta, R. C.; DeLuca, P. P. *Int. J. Pharm.* **1996**, *127*, 43–52.
(44) Croll, T. I.; O'Connor, A. J.; Stevens, G. W.; Cooper-White, J. J. *Biomacromolecules* **2004**, *5*, 463–473.
(45) Biaggi, M. H.; Riske, K. A.; LamyFreund, M. T. *Biophys. Chem.* **1997**, *67*, 139–149.
(46) Serr, A.; Horinek, D.; Netz, R. R. *J. Am. Chem. Soc.* **2008**, *130*, 12408–12413.
(47) Roach, P.; Farrar, D.; Perry, C. C. *J. Am. Chem. Soc.* **2005**, *127*, 8168–8173.
(48) Mu, Y. *Phys. Rev. E* **2011**, *84*, 1–12.
(49) Paragkumar, N. T.; Dellacherie, E.; Six, J. L. *Appl. Surf. Sci.* **2006**, *253*, 2758–2764.
(50) Sahoo, S. K.; Panyam, J.; Prabha, S.; Labhasetwar, V. *J. Controlled Release* **2002**, *82*, 105–114.
(51) Gyulai, G.; Penzes, C. B.; Mohai, M.; Lohner, T.; Petrik, P.; Kurunczi, S.; Kiss, E. *J. Colloid Interface Sci.* **2011**, *362*, 600–606.
(52) Muller, M.; Voros, J.; Csucs, G.; Walter, E.; Danuser, G.; Merkle, H. P.; Spencer, N. D.; Textor, M. *J. Biomed. Mater. Res., Part A* **2003**, *66A*, 55–61.
(53) Richter, R.; Mukhopadhyay, A.; Brisson, A. *Biophys. J.* **2003**, *85*, 3035–3047.
(54) Mornet, S.; Lambert, O.; Duguet, E.; Brisson, A. *Nano Lett.* **2005**, *5*, 281–285.
(55) Keller, C. A.; Kasemo, B. *Biophys. J.* **1998**, *75*, 1397–1402.
(56) Lvov, Y.; Ariga, K.; Ichinose, I.; Kunitake, T. *J. Am. Chem. Soc.* **1995**, *117*, 6117–6123.
(57) Biaggi, M. H.; Pinheiro, T. J. T.; Watts, A.; LamyFreund, M. T. *Eur. Biophys. J.* **1996**, *24*, 251–259.
(58) Schoeler, B.; Sharpe, S.; Hatton, T. A.; Caruso, F. *Langmuir* **2004**, *20*, 2730–2738.
(59) Kolarik, L.; Furlong, D. N.; Joy, H.; Struijk, C.; Rowe, R. *Langmuir* **1999**, *15*, 8265–8275.
(60) Gilles, M. A.; Hudson, A. Q.; Borders, C. L. *Anal. Biochem.* **1990**, *184*, 244–248.
(61) Schoeler, B.; Kumaraswamy, G.; Caruso, F. *Macromolecules* **2002**, *35*, 889–897.
(62) Dubas, S. T.; Schlenoff, J. B. *Macromolecules* **2001**, *34*, 3736–3740.
(63) Garza, J. M.; Jessel, N.; Ladam, G.; Dupray, V.; Muller, S.; Stoltz, J. F.; Schaaf, P.; Voegel, J. C.; Lavalle, P. *Langmuir* **2005**, *21*, 12372–12377.
(64) Schneider, G.; Decher, G. *Langmuir* **2008**, *24*, 1778–1789.